Research Article | Vol. 33, No. 5 / 10 Mar 2025 / Optics Express 11713
Optics EXPRESS

Cost-effective Φ-OTDR with laser phase noise mitigation using self-mixing interferometry

Zhanhang Wei,[1] Yichang Wu,[1,2,4] Tianrui Li,[1] Dajian Cai,[1] Shaoyi Chen,[1] Zhaohui Li,[1,3,5] Dawei Wang,[1,3] and Chao Lu[1,2]

[1]Guangdong Provincial Key Laboratory of Optoelectronic Information Processing Chips and Systems, School of Electronics and Information Technology, Sun Yat-sen University, 510275, Guangzhou, China
[2]Photonics Research Institute, Department of Electrical and Electronic Engineering, The Hong Kong Polytechnic University, Hong Kong SAR, China
[3]Southern Marine Science and Engineering Guangdong Laboratory (Zhuhai), 519082, Zhuhai, China
[4]wuych27@mail2.sysu.edu.cn
[5]lzhh88@mail.sysu.edu.cn

Abstract: The performances and cost of the phase-sensitive optical time-domain reflectometry (Φ-OTDR) systems are heavily influenced by the lasers used. Traditionally, Φ-OTDR systems rely on highly coherent ultra-narrow linewidth lasers (NLL). This paper proposes a Φ-OTDR system that utilizes self-mixing interferometry to mitigate the impact of laser phase noise and a triple-frequency scheme to achieve fading-free detection over 40 km. The proposed scheme employs an inexpensive fixed wavelength distributed feedback semiconductor laser (DFB-SL) with a 93 kHz linewidth as the light source and successfully mitigates the noise floor by 8 to 22 dB within a range of 35 km compared to the performance of conventional systems. Leveraging the high-power output of the DFB-SL, the proposed scheme eliminates the need for an online erbium-doped optical fiber amplifier (EDFA) and achieves fading-free detection over 10 km. The results in this study offer a practical solution to address the bottleneck issue of laser phase noise in Φ-OTDR systems and contribute to the development of cost-effective systems and on-chip integration, eliminating the requirement for NLL and online amplifiers.

1. Introduction

In recent years, distributed fiber acoustic sensing (DAS) has gained prominence due to its exceptional temporal and spatial resolution, extensive sensing range, and high sensitivity to environmental vibrations [1]. Amongst the various methodologies employed, phase-sensitive optical time-domain reflectometry (Φ-OTDR) has been recognized as a key technique in the high-fidelity reconstruction of acoustic signal waveforms [2]. Its high detection sensitivity and long detection range have made Φ-OTDR a valuable tool in applications such as seismic monitoring [3,4], volcanic events detection [5], pipeline leakage detection [6], and other fields.

The performance of Φ-OTDR systems is closely tied to the quality of the laser source, as the interference between local oscillator (LO) light and Rayleigh backscattered (RBS) light is sensitive to laser phase noise, particularly over long distances. This noise, stemming from spontaneous emission, is often characterized by the laser's linewidth. Standard Φ-OTDR setups typically require costly coherent NLL with linewidths bellow 1 kHz. A wider linewidth leads to increased phase noise and reduced system sensitivity [7]. Prior research has demonstrated the critical impact of the laser's instantaneous linewidth on Φ-OTDR sensitivity [8], with various approaches proposed to mitigate laser phase noise, including advanced algorithms and structure. F. Pang et al. have mitigated the impact of laser phase noise using an algorithm that exploits minimal laser phase changes during extremely short periods. However, their work still employed NLL (maximum linewidth of 2.2 kHz) [9]. B. G. Gorshkov et al. employed a self-mixing

#545117 https://doi.org/10.1364/OE.545117
Journal © 2025 Received 21 Oct 2024; revised 13 Jan 2025; accepted 12 Feb 2025; published 5 Mar 2025

Optics EXPRESS

unbalanced Michelson interferometer (MI) to generate dual pulses, reducing the coherence requirements of the laser source [10,11]. Z. He et al. have used an auxiliary interferometer to relax the laser linewidth limitation and realize a linear-frequency-modulation-pulsed (LFMP) Φ-OTDR with 100 kHz linewidth integrable tunable laser assembly [12]. However, the high demands on the stability of the auxiliary interferometer make it difficult to integrate it into the DAS for real environmental measurements. These studies have shown that the laser phase noise has a significant impact on the performances of Φ-OTDR. To mitigate the phase noise of Φ-OTDR systems, the structures such as self-mixing interferometry have been studied. M. Zhang and his team achieved high sensitivity at a detection distance of 470 m using a laser with a linewidth of 200 Hz [13]. They revealed the environment noise suppression of the self-mixing interferometry. However, the scheme of channel sampling for differential frequency signals relies on the highly coherent laser. Y. Zhang et al. utilized a laser with a linewidth of 3.7 kHz and ultra-weak fiber Bragg grating (UWFBG) for high-performance detection in long-range scenarios [14]. Q. Tao et al. studied the suppression of phase fading noise using a dual-pulse Φ-OTDR structure and provided valuable insights into the structure's simulation analysis [15]. L. Shao et al. used a dual-pulse scheme with direct detection to suppress the noise introduced by laser frequency jitter [16]. It is noteworthy that all these investigations utilized NLLs which require a high cost as the light source. The effect of laser phase noise on the performance of Φ-OTDR using self-mixing interferometry is currently unknown and the algorithmically suppressing the phase noise floor based on the self-mixing interferometry is a lack.

In addition, interference fading noise is a critical issue that hinders phase retrieval in Φ-OTDR, especially in the long-range detection. The interference fading noise is caused by the amplitude fluctuation on RBS light traces. When the amplitude of the RBS light falls beneath the noise floor, it is hard to precisely reconstruct the phase signal especially in the self-mixing interferometry scheme in the absence of LO light. Thus, an increasing amount of research has focused on suppressing the fading noise to eliminate "dead zones" in phase recovery. X. Wang et al. applied a 0–π binary phase shift process on the second half of the probing pulse to reduce the probability of interference fading noise [17]. J. Jiang et al. utilized continuous chirped-wave modulation to eliminate fading with the rotated- vector-summation method [18]. M. Zabihi et al. proposed a real-time system with three different probe frequencies to mitigate the fading phenomenon [19]. G. Tu et al. proposed a statistical method based on nearest neighbor analysis to suppress the fading noise caused by phase hopping [20]. These approaches, while effective, either increase the complexity and the cost of the hardware or impose additional restrictions on the algorithms utilized for signal processing. Furthermore, to ensure the coherence between the LO light and the RBS light, these studies also used NLL.

Building on these studies, this paper introduces a novel Φ-OTDR scheme using self-mixing interferometry and novel algorithms to relax the light source's coherence requirements and effectively mitigate the laser phase noise. The triple-frequency scheme with self-mixing interferometry is realized for the first time to counteract interference fading noise and facilitate long-distance, fading-free detection. Using an inexpensive fixed-wavelength distributed feedback semiconductor laser (DFB-SL) with a 93 kHz linewidth, the proposal Φ-OTDR system achieves fading-free detection up to 40 km and the noise floor decreases by 8 dB to 22 dB compared to the conventional systems in the range from 1 km to 35 km. Based on the high-power DFB-SL, the proposal scheme achieves fading-free detection up to 10 km without on-line EDFA. This work provides a feasible scheme for the on-chip Φ-OTDR system without the integration of on-line amplifier.

The paper is organized as follows: Section 2 introduces the principles of the self-mixing interferometry-based Φ-OTDR and the novel algorithms. Section 3 describes the experimental setup. Section 4 discusses the results, highlighting the success of the proposed cost-effective

Optics EXPRESS

scheme in mitigating laser phase noise and suppressing interference fading. The paper concludes with Section 5, summarizing the key findings and contributions.

2. Principle

2.1. Self-mixing interferometry

Laser phase noise is a significant contributor to uncertainties in phase demodulation and the elevation of the noise floor. In the conventional Φ-OTDR structure, the formulation of the beat signal by the heterodyne detection wherein the RBS signal is amalgamated with the LO signal [21], as shown in Eq. (1).

$$I(z,t) \propto Q(z)\cos\left[-2\pi\Delta f t + \varphi(z,t) + \frac{4\pi n}{c} f z + \theta_R(f,z)\right] \tag{1}$$

The term $Q(z)$ represents the amplitude of RBS light, z is the position under consideration, Δf is the beat frequency, $\varphi(z,t)$ is the phase modulated by external perturbation, the symbol n is the refractive index, c is the velocity of light wave in vacuum, f is the optical frequency. The term $\theta_R(f,z)$ represent the phase shift of the reflector at position z and the term of f indicates that $\theta_R(f,z)$ related to the optical frequency f. Due to short period of the probing pulse width in Φ-OTDR, the frequency f in the phase term of $\frac{4\pi n}{c} f z$ and $\theta_R(f,z)$ is considered constant. Considering that the detected electrical signal is actually the accumulation of the optical signal within the pulse width, Eq. (1) is represented as Eq. (2). w is the pulse width.

$$I(z,t) \propto Q(z)\cos[-2\pi\Delta f t] \int_{z}^{z+\frac{w}{2}} \cos\left[\varphi(p,t) + \frac{4\pi n f}{c} p + \theta_R(f,p)\right] dp \tag{2}$$

Due to the variation of the laser frequency introduced by the laser phase noise, the actual beat frequency Δf contains a jitter term for the laser frequency denoted as $\Delta f_{laser}(t)$ and the shift frequency of the AOM denoted as f_{AOM}, as shown in Eq. (3).

$$\triangle f = \Delta f_{laser}(t) + f_{AOM} \tag{3}$$

In this paper, the self-mixing interferometry structure of the Φ-OTDR system realizes the mitigation of laser phase noise. The interference among the probing pulses, which propagate along the same optical path, effectively mitigate the noise originating from the environment. Considering that the phase of the laser only slightly changes during an extremely short period [9], the interference among the RBS light serves to attenuate the influence of laser phase noise. The probing pulses, generated by three acousto-optic modulators (AOMs) with different frequency shifts of f_{AOM1}, f_{AOM2}, f_{AOM3}, have equal pulse width w and repetition frequency f_r. The light wave frequencies of the three probing pulses are f_1, f_2, f_3, respectively. The frequencies of the probing pulses consist of the laser frequency $f_{laser}(t)$ and AOM frequency shifts, which are expressed as $f_i = f_{laser}(t) + f_{AOMi}$ $(i = 1, 2, 3)$. These pulses have specific spatial intervals denoted as L_d as shown in Fig. 1(a). This spatial separation is critical to satisfy the spatial difference operation of Φ-OTDR in the self-mixing interference. Besides, overlapping among the pulses could potentially induce undesirable effects such as variations in the power of RBS light, impacting the system's performance. By ensuring a suitable spatial interval L_d between pulses of different frequencies as shown in Fig. 1(b), the self-mixing interferometry avoids fluctuations in power and maintains the stability of the RBS light. A precise control over the triggers and phases of the three probing pulses is implemented to ensure that the length mismatching of self-mixing interferometry is as close to zero as possible and that the post-interference phases have no modulation phase differences.

Optics EXPRESS

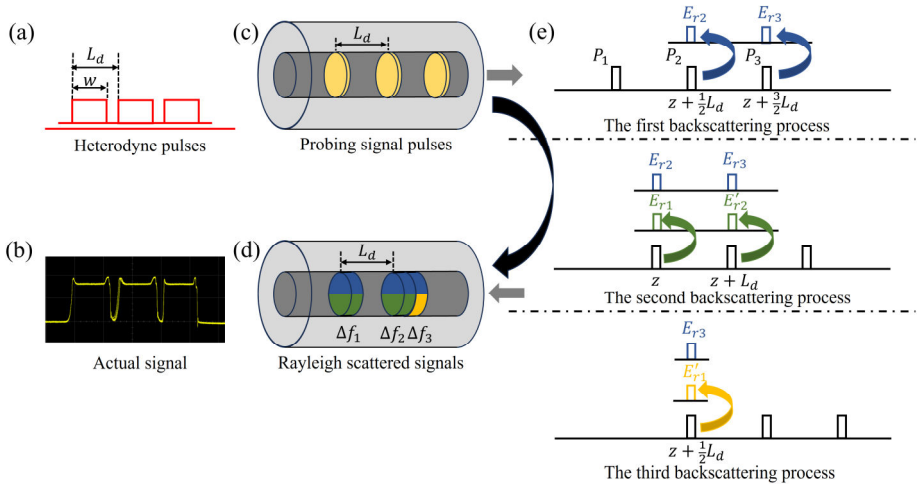

Fig. 1. (a) The probing pulses with equal pulse widths w and repetition frequencies f_r. (b) The actual optical waveform detected by a photodetector. (c) The probing pulses were injected into the fiber. (d) The RBS light corresponds to three interference frequencies. (e) The process of RBS light generation and interference.

The transmission process of probing signal pulses and the interference process of RBS light are also demonstrated in Fig. 1. Figure 1(c) indicates the spatial distribution of the three probing pulses, and Fig. 1(d) indicates the spatial distribution of the RBS light. Figure 1(e) indicates the generation of RBS light by probing pulses along the axial trajectory of the non-uniform optical fiber. As all three probing pulses traverse the same fiber, their noise characteristics bear resemblance to each other. This similarity facilitates a self-cancellation mechanism for the phase noise [22]. The RBS lights of different frequencies interfere with each other at discrete spatial locations. The RBS lights E_{r2} and E_{r3} (corresponding to the frequencies f_2 and f_3) generated at the time of t_1 interfere with the RBS lights E_{r1} and E'_{r2} (corresponding to the frequencies f_1 and f_2) generated at the time of t_2. The interferences produce the signal components at the frequencies of Δf_1 and Δf_2 ($\Delta f_1 = f_2 - f_1$, $\Delta f_2 = f_3 - f_2$). Similarly, the signal component at the frequency of Δf_3 ($\Delta f_3 = f_3 - f_1$) is generated by the interference between the RBS light E_{r3} and the RBS light E'_{r1} generated at the time of t_3. The beat frequency Δf_1, Δf_2, Δf_3 contains the term for the laser frequency jittering denoted as $\Delta f_{laser}(t)$ and the difference between the shift frequencies of the AOMs, as shown in Eq. (4).

$$\begin{aligned} \Delta f_1 &= \Delta f_{laser}(t) + f_{AOM2} - f_{AOM1}, \\ \Delta f_2 &= \Delta f_{laser}(t) + f_{AOM3} - f_{AOM2}, \\ \Delta f_3 &= \Delta f_{laser}(t) + f_{AOM3} - f_{AOM1} \end{aligned} \tag{4}$$

To avoid the spatial overlapping of the RBS light between adjacent detections, the system sends three pulses at a repetition frequency of f_r which is limited by the length of the detection fiber. The expression for the amplitude of the RBS light [15] is provided in Eq. (5). Compared to the self-mixing interferometry with dual-frequency pulses which can only realize single-frequency detection, the triple-frequency scheme realizes multi-frequency detection and effectively

Optics EXPRESS

suppresses the interference fading noise to achieve fading-free detection in long range.

$$\begin{aligned}
&E_{RS}(z,t) = E_{r1} + E_{r2} + E_{r3} \\
&= E_{01} \int_{z}^{z+\frac{w}{2}} r(p) e^{j\theta_R(f_1,p)} e^{-\alpha p} \exp\{j[2\beta p - 2\pi f_1 t + \varphi(p,t)]\} dp \\
&+E_{02} \int_{z+\frac{L_d}{2}}^{z+\frac{L_d+w}{2}} r(p) e^{j\theta_R(f_2,p)} e^{-\alpha p} \exp\{j[2\beta p - 2\pi f_2 t + \varphi(p,t)]\} dp \\
&+E_{03} \int_{z+L_d}^{z+L_d+\frac{w}{2}} r(p) e^{j\theta_R(f_3,p)} e^{-\alpha p} \exp\{j[2\beta p - 2\pi f_3 t + \varphi(p,t)]\} dp
\end{aligned} \tag{5}$$

The amplitudes of the RBS light in three frequencies, denoted as E_{01}, E_{02}, and E_{03}, correspond to frequencies f_1, f_2, and f_3, respectively. The symbol z represents the detection signal at different location channels of the fiber. The spatial distance of z corresponds to the sampling rate of the Φ-OTDR system for a single frame of RBS light. The reflectivity and phase shift of the reflector at position z is represented by $r(z)$ and $\theta_R(f,z)$. And α is the loss coefficient of the sensing fiber, β is the propagation constant of the fiber mod, and t is the time of transmission for each probing pulse in the optical fiber. The term $\varphi(z,t)$ denotes the phase change experienced by the spatial channel z. By utilizing a linear mapping of the phase to strain, the Φ-OTDR system can accurately restore the vibrations of the fiber [23].

To simplify the expression and computation, $Q(z)$ is used to represent the amplitude of RBS light E, the reflectivity of the reflector $r(z)$ and the loss coefficient $e^{-\alpha z}$ ($Q(z) = E \cdot r(z) \cdot e^{-\alpha z}$). Note that the phase shift of the reflector is still represented by $\theta_R(f,z)$ in the exponential term. Substitute into the expression for the propagation coefficient $\beta = 2\pi nf/c$. The expression for the simplified Eq. (5) is provided in Eq. (6).

$$\begin{aligned}
&E_{RS}(z,t) = E_{r1} + E_{r2} + E_{r3} \\
&= Q_1(z)\exp\{j[-2\pi f_1 t]\} \int_{z}^{z+\frac{w}{2}} \exp\left\{j\left[\theta_R(f_1,p) + \tfrac{4\pi n f_1}{c} p + \varphi(p,t)\right]\right\} dp \\
&+Q_2(z)\exp\{j[-2\pi f_2 t]\} \int_{z+\frac{L_d}{2}}^{z+\frac{L_d+w}{2}} \exp\left\{j\left[\theta_R(f_2,p) + \tfrac{4\pi n f_2}{c} p + \varphi(p,t)\right]\right\} dp \\
&+Q_3(z)\exp\{j[-2\pi f_3 t]\} \int_{z+L_d}^{z+L_d+\frac{w}{2}} \exp\left\{j\left[\theta_R(f_3,p) + \tfrac{4\pi n f_3}{c} p + \varphi(p,t)\right]\right\} dp
\end{aligned} \tag{6}$$

In the process of detecting the RBS light, a Sagnac self-interference structure is used to ensure the correctness of symbols for the electrical signals converted by photodetectors. The structure of Sagnac self-interference is shown in Fig. 2.

The RBS light E_{Rs} is computed by the transfer function of a 2×2 optical coupler for the first time as shown in Eq. (7) and is computed by the transfer function of a 2×2 optical coupler for the second time as shown in Eq. (8). The phase term φ_{del} is introduced by the phase change of the optical signals E_{out1} and E_{out2} for the propagation through the self-interference structure, which is a constant that can be easily eliminated in the digital domain. Since the light travels through the same modulated optical path, in practical applications, a stable output signal can be obtained with just a minor encapsulation of the interferometer.

$$\begin{bmatrix} E_{out1} \\ E_{out2} \end{bmatrix} = \frac{\sqrt{2}}{2} \begin{bmatrix} 1 & j \\ j & 1 \end{bmatrix} \begin{bmatrix} E_{RS} \\ 0 \end{bmatrix} = \frac{\sqrt{2}}{2} \begin{bmatrix} E_{RS} \\ jE_{RS} \end{bmatrix} \tag{7}$$

Optics EXPRESS

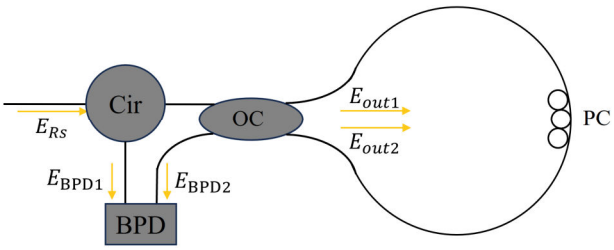

Fig. 2. The self-interference structure of the Sagnac self-interferometer. Cir: Circulator, OC: optical coupler, PC: polarization controller.

$$\begin{aligned}\begin{bmatrix} E_{BPD1} \\ E_{BPD2} \end{bmatrix} &= \frac{\sqrt{2}}{2}\begin{bmatrix} 1 & j\cdot e^{j\varphi_{del}} \\ j\cdot e^{j\varphi_{del}} & 1 \end{bmatrix}\begin{bmatrix} E_{out1} \\ E_{out2} \end{bmatrix} \\ &= \frac{1}{2}\begin{bmatrix} 1 & j\cdot e^{j\varphi_{del}} \\ j\cdot e^{j\varphi_{del}} & 1 \end{bmatrix}\begin{bmatrix} E_{RS} \\ jE_{RS} \end{bmatrix} \\ &= \frac{1}{2}\begin{bmatrix} E_{RS} - E_{RS}\cdot e^{j\varphi_{del}} \\ j\cdot E_{RS} + j\cdot E_{RS}\cdot e^{j\varphi_{del}} \end{bmatrix}\end{aligned} \tag{8}$$

To mitigate common-mode noise in the optical signals, this paper employs a balanced photodetector (BPD) for photoelectric conversion. The relative intensity noise (RIN) received by the two photodiodes is correlated, and the RIN stemming from the laser's optical power instability is canceled out through the differencing process of the two photocurrents [24]. The electrical signals I_{in1} and I_{in2}, which are photoelectrically converted by the BPD, are proportional to the square of the amplitude of the optical signals E_{BPD1} and E_{BPD2} as depicted in Eq. (9). The final electrical signal I_{BPD} is obtained from the difference between I_{in1} and I_{in2} as shown in Eq. (10).

$$\begin{bmatrix} I_{in1} \\ I_{in2} \end{bmatrix} \propto \begin{bmatrix} |E_{BPD1}|^2 \\ |E_{BPD2}|^2 \end{bmatrix} \propto \begin{bmatrix} |1 - e^{\varphi_{del}}|^2 \cdot |E_{RS}|^2 \\ |j + je^{\varphi_{del}}|^2 \cdot |E_{RS}|^2 \end{bmatrix} \tag{9}$$

$$\begin{aligned} I_{BPD} &= I_{in1} - I_{in2} \\ &\propto [|1 - e^{j\varphi_{del}}|^2 - |1 + e^{j\varphi_{del}}|^2] \cdot |E_{RS}|^2 \\ &\propto -2\cos(\varphi_{del}) \cdot |E_{RS}|^2 \end{aligned} \tag{10}$$

It is noteworthy that in the absence of a self-interference structure before the BPD, the electrical signals (I_{in1} and I_{in2}) exhibit identical magnitudes and signs, leading to a mutual cancellation of the resultant differential signals and thus failing to accurately capture the RBS light E_{RS}. Furthermore, the Sagnac interferometer ensures that the light beams traverse through identical optical paths and subsequently enter the BPD. The implementation of a Sagnac interferometer can enhance the stability of the electrical signal than other self-interference structures, like Mach-Zehnder structures [24]. Deviations in the optical path lengths introduce a delay term, resulting in the filtering of the signal spectrum with a free spectral range (FSR). The FSR ΔF is determined by the optical path difference ΔL as shown in Eq. (11), where c represents the speed of light in a vacuum and n represents the refractive index of the fiber.

$$\triangle F = \frac{c}{n\cdot\ \triangle L} \tag{11}$$

Optics EXPRESS

It is important to consider the effect of the FSR on signal quality. When the carrier frequency of the signal falls within the spectral depression, the signal amplitude is reduced and the demodulation phases have a large deviation. Conversely, when the optical path difference ΔL is zero, the FSR ΔF approaches infinity, resulting in a uniform signal spectrum. The spectral flatness would ensure the signal-to-noise ratio (SNR) and demodulation phase quality of the triple-frequency components.

Substituting the expression for RBS light in Eq. (5) into Eq. (10). Considering the low-pass detection characteristics of the BPD [25] and removing the DC component from the signal and unify the starting point of the integral to z, the expression for the final acquired signal of the system is obtained, as shown in Eq. (12).

$$\begin{aligned}
I(z,t) \propto\ & Q_1(z)Q_2(z)\cos[-2\pi\triangle f_1 t]\int_z^{z+\frac{w}{2}}\cos\left[\begin{array}{l}\varphi(p+\frac{1}{2}L_d,t)-\varphi(p,t)+\\ \frac{4\pi n f_2}{c}\left(p+\frac{1}{2}L_d\right)-\frac{4\pi n f_1}{c}p+\theta_R\left(f_2,p+\frac{1}{2}L_d\right)-\theta_R(f_1,p)\end{array}\right]dp\\
+& Q_2(z)Q_3(z)\cos[-2\pi\triangle f_2 t]\int_z^{z+\frac{w}{2}}\cos\left[\begin{array}{l}\varphi(p+\frac{3}{2}L_d,t)-\varphi(p+L_d,t)+\\ \frac{4\pi n f_3}{c}\left(p+\frac{3}{2}L_d\right)-\frac{4\pi n f_2}{c}(p+L_d)+\theta_R\left(f_3,p+\frac{3}{2}L_d\right)-\theta_R(f_2,p+L_d)\end{array}\right]dp\\
+& Q_3(z)Q_1(z)\cos[-2\pi\triangle f_3 t]\int_z^{z+\frac{w}{2}}\cos\left[\begin{array}{l}\varphi(p+\frac{3}{2}L_d,t)-\varphi(p+\frac{1}{2}L_d,t)+\\ \frac{4\pi n f_3}{c}\left(p+\frac{3}{2}L_d\right)-\frac{4\pi n f_1}{c}\left(p+\frac{1}{2}L_d\right)+\theta_R\left(f_3,p+\frac{3}{2}L_d\right)-\theta_R\left(f_1,p+\frac{1}{2}L_d\right)\end{array}\right]dp
\end{aligned} \tag{12}$$

$I(z,t)$ is obtained from the pairwise interference of E_{R1}, E_{R2}, E_{R3} in $E_{RS}(z,t)$ as given by Eq. (6). The term $-2\pi\Delta f_i t$ $(i=1,2,3)$ represent the carrier frequency interference terms, and the corresponding relationship of the interference frequency Δf_i is shown in Eq. (4). $\varphi(z,t)$ represents the phase change experienced by the interference results at different position z. The last four terms respectively represent the interference results of the propagation constant $2\beta z$ and the phase shift of the reflector $\theta_R(f,z)$ at different position z. Here, L_d denotes the spatial interval between pulses of different frequencies.

It is observed that phase terms of Φ-OTDR signal using self-mixing interferometry corresponds to the phase terms of the conventional Φ-OTDR, as shown in Eq. (2). The signal of self-mixing interferometry is already spatially differentiated during the optical interference process [13]. In contrast, the signal of the conventional structure still needs to be spatially differentiated in the digital domain with respect to the phase.

To analyze the laser jitter frequency $\Delta f_{laser}(t)$ present in the frequency term of the signals of the two structures, the laser phase noise $\theta_{lpn}(t)$ is used to denote the phase change introduced by the laser frequency jittering. To evaluate the impact of laser phase noise on the noise floor of Φ-OTDR systems, it is necessary to analyze the numerical effects of linewidth and length mismatch between interfering light. The laser phase noise induced by linewidth is expressed as $\varphi_n(t)$ [26]. The laser phase noise $\varphi_n(t)$ for a Lorentzian-shaped laser linewidth can be described as a random walk Wiener process, as shown in Eq. (13). In this Wiener process, ε_m are independently zero-mean Gaussian distributed random variables with a variance of σ^2, and $k = t/T_s$, where T_s is the symbol period, and $\sigma^2 = 2\pi\Delta\nu T_s$, where $\Delta\nu$ is the laser linewidth.

$$\varphi_n(t)_{t=kT_s} = \sum_{m=-\infty}^{m=k}\varepsilon_m \tag{13}$$

In a coherent detection system, the length mismatch ΔL between the received optical signal ($E_s(t)$, which is the RBS light signal in Φ-OTDR) and reference optical signal ($E_{ref}(t)$, which is the LO light signal in the conventional Φ-OTDR and the RBS light signal in the proposed Φ-OTDR) considered. The detected signal can be expressed as $E_s(t)E^*_{ref}(t-\tau_{\Delta L})$, where $\tau_{\Delta L} = n\cdot\frac{\Delta L}{c}$ is the delay mismatch in time. The laser phase noise $\theta_{lpn}(t)$ can be expressed as the phase of the

Optics EXPRESS

detected signal in coherent detection system, as shown in Eq. (14).

$$\theta_{lpn}(t) = 2\pi f_c \tau_{\triangle L} + \varphi_n(t) - \varphi_n(t - \tau_{\triangle L}) \tag{14}$$

Equation (13) is brought into Eq. (14) to obtain the relationship between the laser phase noise of in Φ-OTDR and laser linewidth, as shown in Eq. (15).

$$\theta_{lpn}(t) = 2\pi f_c \tau_{\triangle L} + \sum_{m=-\infty}^{m=t/T_s} \varepsilon_m - \sum_{m=-\infty}^{m=(t-\tau_{\triangle L})/T_s} \varepsilon_m = \begin{cases} 2\pi f_c \tau_{\triangle L}, \tau_{\triangle L} = 0 \\ 2\pi f_c \tau_{\triangle L} + \sum_{m=(t-\tau_{\triangle L})/T}^{m=t/T} \varepsilon_m, \tau_{\triangle L} \neq 0 \end{cases} \tag{15}$$

To characterize the impact of laser phase noise on the Φ-OTDR noise floor, the power spectral density (PSD) $P_{\theta_{lpn}}(f)$ of laser phase noise $\theta_{lpn}(t)$ is calculated with DC term removed. This is done by taking the Fourier transform and squaring result, as shown in Eq. (16).

$$P_{\theta_{lpn}}(f) = P_{\varphi_n}(f)|H(f)|^2 \tag{16}$$

The PSD of the phase noise $\varphi_n(t)$ introduced by the linewidth is expressed as $P_{\varphi_n}(f)$ and given by $P_{\varphi_n}(f) = \Delta v/(2\pi f^2)$ [27], and the transfer function of the differential operation with interval time $\tau_{\Delta L}$ is denoted as $H(f) = 1 - \exp(-j2\pi f \tau_{\Delta L})$. In the conventional Φ-OTDR system, the final phase results are spatially differentiated, so the spatially difference transfer function is also needed to calculate the noise floor of Φ-OTDR system, as shown in Eq. (17). The transfer function of spatial difference is expressed as $H_s(f) = 1 - \exp(-j2\pi f \tau_{L_d})$, where τ_{L_d} is the spatial delay in time.

$$\begin{aligned} P'_{\theta_{lpn}}(f) &= P_{\varphi_n}(f)|H(f)H_s(f)|^2 \\ &= \tfrac{\triangle \nu}{2\pi f^2}|[1 - \exp(-j2\pi f \tau_{\triangle L})][1 - \exp(-j2\pi f \tau_{L_d})]|^2 \end{aligned} \tag{17}$$

Observing Eq. (17), as the laser linewidth Δv increases, the noise floor $P'_{\theta_{lpn}}(f)$ of Φ-OTDR also increases. By decreasing the delay mismatch in time $\tau_{\Delta L}$, the PSD of laser phase noise $P'_{\theta_{lpn}}(f)$ can be reduced. In the self-mixing interferometry Φ-OTDR, the magnitude of ΔL is relatively small, resulting in significant mitigation of $P'_{\theta_{lpn}}(f)$. To illustrate the relationship between the laser phase noise of Φ-OTDR and the laser linewidth Δv, we can simulate it. The Φ-OTDR signals of single channel is the down-sampling results of the high-frequency analog-to-digital converter (ADC) data. Assuming that the ADC sampling rate is 1 GHz and the repetition frequencies f_r is 2 kHz, the final signals of single channel is an aliasing of spectral densities within the range of 500 MHz in the range of 1 kHz with an interval of 2 kHz. As shown in Fig. 3(a), the amplitude spectral density of the laser phase noise with different linewidths is normalized as 1. The noise floor of Φ-OTDR increases as the laser linewidth broadens.

To observe the trend of laser phase noise along the detection distance of Φ-OTDR, the PSD of laser phase noise at different locations is calculated. Figure 3(b) shows the laser noise floor with different linewidths Δv and different mismatching lengths ΔL. In the conventional Φ-OTDR with the length match ΔL equal to twice the detection distance, the blue and red lines indicate the substantial degradation of laser phase noise introduced by the laser linewidth. In Φ-OTDR using self-mixing interferometry, the length match ΔL depends only on the small difference in optical range in front of the different modulators on the hardware system, which is negligible compared to the detection range. The green line in Fig. 3(b) indicates that the laser phase noise of self-mixing interferometry is not significantly degraded even with a large laser linewidth and the laser noise floor $P_{\theta_{lpn}}(f)$ is mitigated. Note that the laser phase floors of Φ-OTDR do not change as the detection distance increases in the kilometer scale because the coefficient before the ΔL of the high-frequency part is large. The down-sampling results in the laser phase noise after spectral

Optics EXPRESS

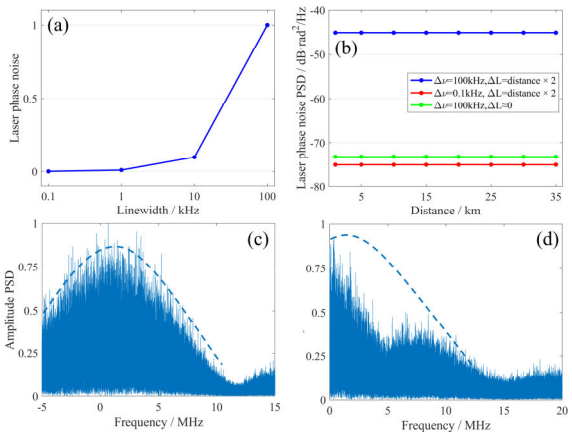

Fig. 3. (a) The relationship between the laser phase noise and laser linewidth. (b) The relationship between the laser phase noise and distance with different linewidths and lengths mismatch. (c) The spectrum of the optical signal with interference frequency near zero frequency. (d) The spectrum of the detected signal by BPD.

aliasing being insensitive to the change of ΔL in the kilometer scale. In this simulation, we only discuss the effect of laser phase noise on the noise floor. The environmental noise or intensity noise is out of scale. In the actual Φ-OTDR system, as the detection distance increase, the phase noise floor rises because of the signal strength reduction due to transmission loss, which affects the SNR of the demodulated phase.

Due to the square wave modulation of the probing pulses, the spectrum of interference signals between the RBS light broadens as the pulse width decreases. At the same time, as the probing pulses enter the fiber under test (FUT) through the gain of the EDFA, the higher gain power also leads to the nonlinear effect caused by the broadening of the spectrum. Given that the BPD only detects the intensity of the optical signal, the signal acquired by the system is a superposition of positive and negative frequencies, containing information and the complex conjugated of information about the beating of the RBS light. The superposition of positive and negative corresponds to the absolute value of the spectrum and does not affect the demodulation of the information. However, when the signal spectrum is located near the zero frequency, which is the demarcation line between the positive and negative frequencies, spectral aliasing occurs, resulting in signal distortion. This phenomenon has been verified in simulation experiments based on Eq. (5), as shown in Fig. 3(c) and (d). Specifically, Fig. 3(d) shows the spectral distortion due to aliasing of positive and negative frequencies of the optical signal spectrum in Fig. 3(c). To mitigate this issue, the modulation scheme is designed to ensure that the minimum interference frequency of $f_{AOM2} - f_{AOM1}$ is set significantly above zero, thereby suppressing the effects of spectrum aliasing.

2.2. Demodulation and algorithm

In this study, an algorithmic to further mitigate the phase noise arising from the phase demodulation process for self-mixing interferometry Φ-OTDR is implemented. To extract the phase information, IQ demodulation, and low-pass filtering techniques are employed. After IQ demodulation, the phase of the detected signal shown in Eq. (12) is obtained after removing the frequency term. The phases of triple frequency components are denoted as θ_1, θ_2 and θ_3. Figure 1(e) reveals that spans of spatial difference between the interference signal at different frequencies are different. The superposition and translation in the spatial domain are calculated to compensate for these spatial separations. The operation ensures that signals with different frequencies correspond to

Optics EXPRESS

the same spatial channels as shown in Eq. (18). The arrow sign represents the correspondence relationship on the spatial channel.

$$\theta_1(z+L_d)-\theta_1\left(z+\frac{1}{2}L_d\right) \overset{Spatial}{\longleftrightarrow} \theta_2(z)-\theta_2\left(z-\frac{1}{2}L_d\right) \overset{Spatial}{\longleftrightarrow} \theta_3(z) \tag{18}$$

As shown in Eq. (12), to obtain the phase modulated by external perturbation $\varphi(t)$, it is necessary to eliminate the phase shift of the reflector $\theta_R(z)$ and the propagation phase shift $\frac{2\pi nf}{c}z$. They are small phase variations with an interval of L_d, and since they are not related to the time t, they can be eliminated through phase initialization in the large time domain. The conventional phase initialization method uses the result of the first probing as the initial phase, which contains the phase error of the first detection frame. An innovative phase initialization methodology utilizing complex vectors across time and frequency domains is employed to eliminate phase errors. The in-phase and quadrature signals for different frequencies are shown in Fig. 4(a). This methodology considers the phase variation between different pulses on the same spatial channels [28] and utilizes scalar averaging of the phase variation term of different frequencies, as shown in Eq. (19,20) and Fig. 4(b).

$$\begin{bmatrix} E_{RS1} \\ E_{RS2} \\ E_{RS3} \end{bmatrix} = \begin{bmatrix} A\exp(\varphi_1) & \dots & A\exp(\varphi_1^n) \\ A\exp(\varphi_2) & \dots & A\exp(\varphi_2^n) \\ A\exp(\varphi_3) & \dots & A\exp(\varphi_3^n) \end{bmatrix} \tag{19}$$

$$\begin{bmatrix} \triangle\varphi^2 \\ \dots \\ \triangle\varphi^n \end{bmatrix} = \begin{bmatrix} \frac{1}{3}\sum_{i=1}^{3}(\varphi_i^2-\varphi_i) \\ \dots \\ \frac{1}{3}\sum_{i=1}^{3}(\varphi_i^n-\varphi_i) \end{bmatrix} \tag{20}$$

To simplify the computational expression, the signal amplitudes are denoted by A, the phases of the vector signals are denoted by φ, the symbol subscripts represent the three different frequency components, and the symbol superscripts indicate the numbering of probing pulses in the time domain. After calculation, we obtain the scalar average time-domain phase difference $\Delta\varphi$ of the three frequency signals. Then, the initial phase $\varphi^{initial}$ is calculated by vectorial summation of the rotated vector, as demonstrated in Eq. (21).

$$\begin{bmatrix} \varphi_1^{initial} \\ \varphi_2^{initial} \\ \varphi_3^{initial} \end{bmatrix} = \begin{bmatrix} \angle\left\{\frac{1}{n}\sum_{i=1}^{n}[A\exp(\varphi_1^i-\Delta\varphi^i)]\right\} \\ \angle\left\{\frac{1}{n}\sum_{i=1}^{n}[A\exp(\varphi_2^i-\Delta\varphi^i)]\right\} \\ \angle\left\{\frac{1}{n}\sum_{i=1}^{n}[A\exp(\varphi_3^i-\Delta\varphi^i)]\right\} \end{bmatrix} \tag{21}$$

$\angle$ denotes the angle of the resulting averaged vector. By employing vector averaging, a more accurate initial vector angle can be obtained, weighted by the vector magnitudes. The process of vector summation for the initial phase $\varphi^{initial}$ is shown in Fig. 4(c). The algorithm ensures that vectors of three frequencies match each other and eliminate the initial phase error in the time domain. The initialization operation is performed on the signal matrix in the time domain based

Optics EXPRESS

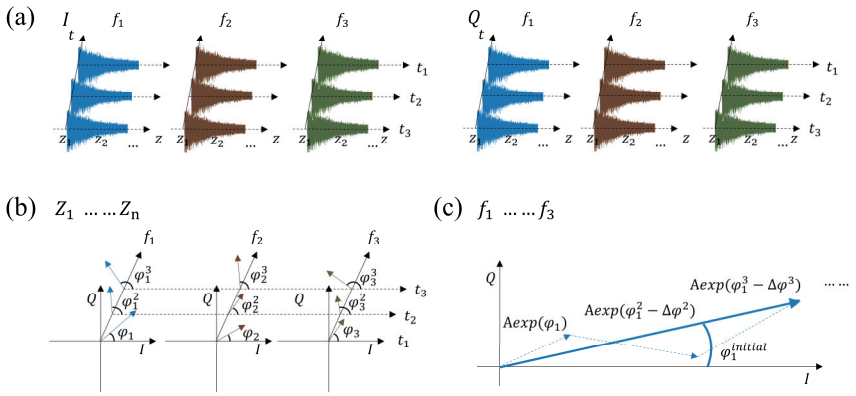

Fig. 4. The signal processing methodology of complex vectors. (a) The in-phase and quadrature signals for different frequencies. (b) The phase variation between different pulses on the same spatial channel. (c) The summation of the rotated vectors for obtaining the initial vectors in the time domain.

on the initial vectors, as shown in Eq. (22).

$$\begin{bmatrix} E'_{RS1} \\ E'_{RS2} \\ E'_{RS3} \end{bmatrix} = \begin{bmatrix} A\exp(\varphi_1 - \varphi_1^{\text{initial}}) \ldots A\exp(\varphi_1^{\text{n}} - \varphi_1^{\text{initial}}) \\ A\exp(\varphi_2 - \varphi_2^{\text{initial}}) \ldots A\exp(\varphi_2^{\text{n}} - \varphi_2^{\text{initial}}) \\ A\exp(\varphi_3 - \varphi_3^{\text{initial}}) \ldots A\exp(\varphi_3^{\text{n}} - \varphi_3^{\text{initial}}) \end{bmatrix} \tag{22}$$

Compared to the E_{RS} in Eq. (19), E'_{RS} in Eq. (22) has a smaller phase error across frequencies, especially for small amplitude signals. Finally, by rotated vector sum of the triple-frequency components, the phase demodulation process achieves weighted averaging. Owing to the fact that the initial phase exhibits distinct errors for different components, the conventional rotated vector sum algorithm solely utilizes the first detected pulse as the initial phase, thereby introducing random error noise upon combination. In contrast, the innovative phase initialization methodology presented in this work, by integrating both the frequency domain and the time domain, calculates a more accurate initial phase. Consequently, this enhances the degree of phase matching for different component signals during the computation process of the rotated vector sum. The phase error due to low magnitude at a single frequency can be compensated, and the interference fading noise can be effectively suppressed.

By utilizing the aforementioned hardware system of Φ-OTDR based on self-mixing interferometry, accurate restoration of the phase variations $\varphi(z, t)$, which map the environmental vibrations, can be achieved. By innovative phase initialization methodology utilizing complex vectors across time and frequency domains and rotated vector sum, the interference of fading noise in the recovery of phase variations is suppressed, allowing accurate restoration results to be presented at all positions along the optical fiber.

3. Experimental setup

The experimental setup for the proposed novel Φ-OTDR system using self-mixing interferometry is demonstrated in Fig. 5(a).

The light sources used for the experiment include the NLL (NKT E15) with a 0.1 kHz ultra-narrow linewidth and the DFB-SL with a 93 kHz linewidth, which are used to characterize systems with low and high laser phase noise, respectively. The DFB-SL with an output optical power of 82 mW served as the light source. The continuous light emitted by the laser was modulated by

Optics EXPRESS

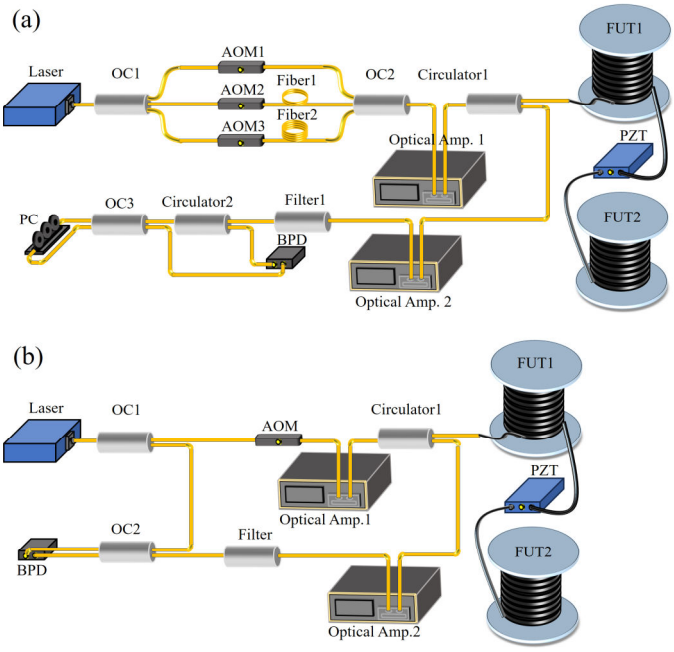

Fig. 5. System setup. (a) The structure of the proposal Φ-OTDR system. (b) The structure of the conventional Φ-OTDR system. OC: optical coupler, AOM: acousto-optic modulator, FUT: fiber under test, PZT: piezoelectric transducer, PC: polarization controller.

three AOMs to generate probing pulses with a pulse width of 100 ns. The AOMs were configured to shift the light source at the frequencies of 80 MHz (negative frequency shifting), 80 MHz (positive frequency shifting), and 200 MHz (positive frequency shifting), respectively. The delay fibers are set after AOM2 and AOM3 to separate the pluses and the length of delay fibers are 20 m and 40 m, respectively. An on-line EDFA (Amonics, AEDFA-23-M-FA) is used for the probing pulses gaining when the length of FUT is 40 km and there is no on-line EDFA when the DFB-SL is used and the length of FUT is 10 km. To ensure the RBS trace of adjacent interrogation will not overlap, the pulse repetition frequency is set to 2 kHz or 8 kHz corresponding to the FUT of 40 km or 10 km. And the gauge length is set to 20 meters. To simulate vibration events, a piezoelectric transducer (PZT) driven by an arbitrary waveform generator (AWG) was placed at the distance of 39.5 km or 9.5 km from the system. The length of the fiber wrapped around the PZT is 15 m. The RBS lights generated along the FUT passed through an EDFA (Amonics, AEDFA-PA-30-M-FA), an optical filter, and a Sagnac interferometry comprising an optical coupler (OC), a circulator, and a fiber polarization controller (PC). Subsequently, the RBS light was detected by a BPD with a bandwidth of 500 MHz. Finally, the system recovered the phase information from the electrical signals output by the BPD.

The conventional structure has the LO light involved in the interference, which is shown in Fig. 5(b). The same lasers are used as the light source and the same AOM at the frequency shifting of 200 MHz are used for the modulation. The probing pulse propagates the same FUT and the RBS light is detected by the same BPD after the interference with the LO light.

4. Results and discussion

The NLL with 0.1 kHz ultra-narrow linewidth is used to characterize the lowest noise floor of Φ-OTDR with different schemes. Figure 6(a) shows the consecutive phase traces along the FUT

Optics EXPRESS

recovered by the conventional Φ-OTDR scheme where the curves with different colors represent the phases with different probing pulses for a period of 100 milliseconds. The phase traces show that there is a phase change only at 39.5 km where the PZT is located, and the rest of the phase is vibration-free system noise. The phase noise floors at different positions recovered by the conventional Φ-OTDR is shown in Fig. 6(b). To avoid serendipity in the comparison, phases with a duration of 4 seconds (corresponding to 8,000 probing pulses) and a span of 100 meters are used to calculate the average PSD. The frequency spikes below 50 Hz are caused by environmental noise. Figure 6(c) and (d) show the consecutive phase traces and phase noise floors of the proposal Φ-OTDR. The average phase noise at different positions is averaged from 100 Hz to 1000 Hz and the comparison of the phase noise floors along the FUT between the conventional scheme and the proposal scheme is shown in Fig. 6(e). It can be observed that the phase noises of the systems show a positively correlated increase with the distance which is the combined result of transmission loss. The decrease in detection power caused by optical transmission loss leads to the decrease in SNR [29]. The phase noise between the conventional scheme and the proposal scheme is close to each other at different locations. The noise floor of the proposal scheme at 1 km is -66 $dB \cdot rad^2/Hz$ (converted to the unit of 8 $dB \cdot p\varepsilon^2/Hz$), and the noise floor at 35 km is -53 $dB \cdot rad^2/Hz$ (converted to the unit of 21.2 $dB \cdot p\varepsilon^2/Hz$) which are at the leading edge of current schemes.

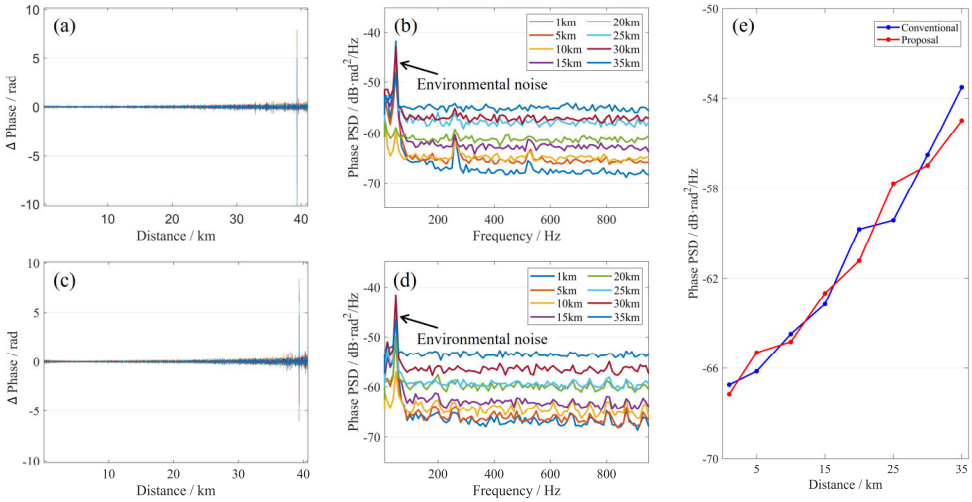

Fig. 6. The noise floor of Φ-OTDR using the NLL with the conventional scheme and proposal scheme. (a) The consecutive phase traces along the FUT with the conventional Φ-OTDR. (b) The phase noise floor at different positions of conventional Φ-OTDR. (c) The consecutive phase traces along the FUT with the proposal Φ-OTDR. (d) The phase noise floor at different positions of proposal Φ-OTDR. (e) The phase noise floor along the FUT.

To characterize the mitigation for the laser phase noise, the DFB-SL with a 93 kHz linewidth is used as the light source for the same comparison, as shown in Fig. 7. Figure 7(a) and (b) show the consecutive phase traces and phase noise floors of the conventional Φ-OTDR scheme, Fig. 7(c) and (d) show the consecutive phase traces and phase noise floors of the proposal Φ-OTDR scheme. The solid lines in Fig. 7(e) show phase noise along the FUT with the conventional scheme and proposal scheme using the DFB-SL as light source, where the dashed lines are the curves using the NLL as light source which have shown in Fig. 6(e) for easy comparison. It shows that the proposal scheme still exhibits the tendency of the phase noise floor increasing with the detection distance, while the conventional scheme is affected by the laser phase noise which is high at every position. The trend of the blue solid line is consistent with the simulation

Optics EXPRESS

results of laser phase noise in Section 2 and the trend of the red solid line is due to the decrease in detection power caused by transmission loss. The noise floor degradation of the proposal scheme introduced by the laser phase noise using DFB-SL as light source is less than 3 dB in the range of 35 km compared to the light source with NLL. Compared to the conventional scheme which is degraded by laser phase noise, the noise floor of the proposal scheme is 22 dB lower at the position of 1 km and 8 dB lower at the position of 35 km. The results indicate that when the linewidth is large, the noise floor of conventional Φ-OTDR is heavily affected by the laser phase noise. The Φ-OTDR using self-mixing interferometry effectively mitigates the laser phase noise by more than 8 dB at 35 km. And the noise floors along the FUT of the system using self-mixing interferometry are still affected by the transmission loss, which show the increase with the distance.

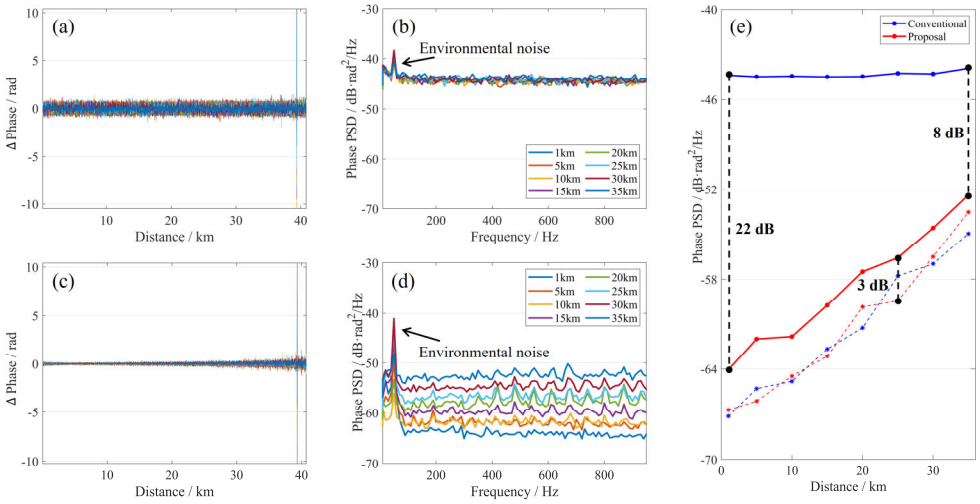

Fig. 7. The noise floor of Φ-OTDR using DFB-SL with the conventional scheme and proposal scheme. (a) The consecutive phase traces along the FUT with the conventional Φ-OTDR. (b) The phase noise floor at different positions of the conventional Φ-OTDR. (c) The consecutive phase traces along the FUT with the proposal Φ-OTDR. (d) The phase noise floor at different positions of the proposal Φ-OTDR. (e) The phase noise floor along the FUT (the dashed lines show the noise floor curves in Fig. 6(e)).

To further observe the effect of the self-mixing interferometry scheme on the recovery of vibration waveform and the suppression of interference fading noise with triple-frequency detection, a sinusoidal radio frequency (RF) signals with a frequency of 200 Hz and a voltage amplitude of 0.3 V are generated as the PZT vibration at the position of 39.5 km. A comparison is made between the vibration recovery by the conventional scheme and the proposal scheme using DBF-SL. The time-domain waveforms of the recovered phases are shown in Fig. 8. Figure 8(a) shows the recovered phases of the conventional scheme, and Fig. 8(b) shows the recovered phases of the proposal scheme. It can be observed that the phases of the conventional scheme show the distortion of jittering at the time of 0.04 s and 0.06 s. In contrast, the phases recovered by the proposal scheme demonstrate better fidelity, which is the joint result of the self-mixing structure mitigating laser phase noise and the innovative rotated vector sum suppressing fading noise.

Figure 8(c), (d) and (e) show the consecutive phase traces along the FUT recovered by the single-frequency, dual-frequency and triple-frequency schemes. Each plot contains the phase traces with the number of 200 (corresponding to the pulses with a duration of 100 milliseconds). Each colored trace represents the phase variations obtained by demodulating the RBS light of each probing pulse. Figure 8(c) exhibits a significant amount of phase errors after the position

Optics EXPRESS

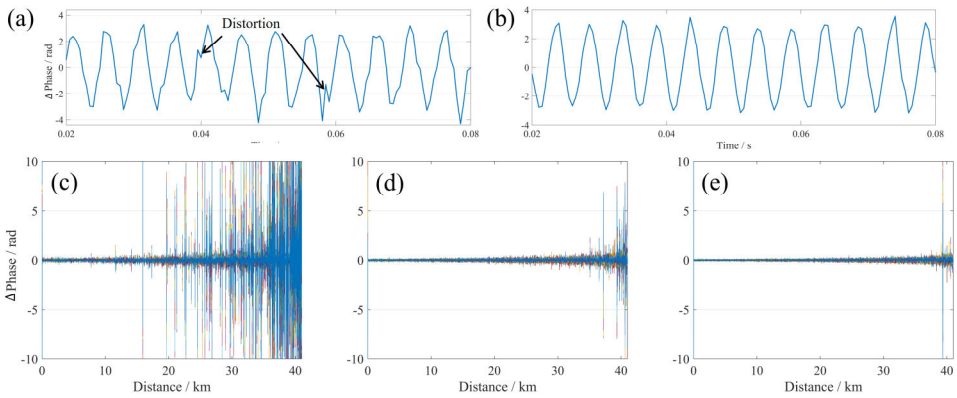

Fig. 8. The recovered phases at the location of the PZT and the consecutive phase traces along the FUT. The recovered phases at the location of the PZT with (a) the conventional structure and (b) the proposal structure. The consecutive phase traces along the FUT with (c) single-frequency, (d) dual-frequency and (e) triple-frequency.

of 15 km, which affect the judgment and restoration of the actual environmental vibration. As illustrated in Fig. 8(d) and (e), the phase errors begin to appear at the position of 35 km in the dual-frequency scheme and only the vibration of PZT at the position of 39.5 km remains in the triple-frequency scheme. It shows that the self-mixing interferometry Φ-OTDR with triple-frequency scheme is effective in suppressing the interference fading noise. The probability of interference fading noise decreases with the increase of frequency components in the scheme [30,31]. This is also the first time that a large detection range of 40 km has been realized in a Φ-OTDR system based on a self-mixing interferometry structure without inline optical amplification.

To realize a more cost-effective Φ-OTDR system and for the trend of on-chip Φ-OTDR with non-integrable optical amplifiers, this work achieves the detection range of 10 km without on-line EDFA. Based on the high-power optical output characteristics of DFB-SL, a Φ-OTDR scheme using self-mixing interferometry for easy on-chip integration is provided. In the absence of on-line EDFA, the noise floor of the self-mixing interferometry structure at the position of 9 km is 8 dB lower compared to the conventional scheme, as shown in Fig. 9(a). Figure 9(b) and (c) shows the consecutive phase traces along the FUT with the triple-frequency detection and single-frequency detection. The phase errors caused by the interference fading noise are suppressed and only the phase changes caused by the stretching of the PZT occur at the position of 9.5 km, as shown in Fig. 9(c).

The amplitude-frequency characteristic of the scheme without on-line EDFA is discussed in this work. The amplitude-frequency characteristic reflects the responses of the Φ-OTDR system to the vibrations of different frequencies and amplitudes. A sinusoidal signal is generated with the amplitude ranging from 0.2 V to 4.6 V, and the frequency ranging from 20 Hz to 460 Hz. The sinusoidal signal is loaded onto the PZT to simulate environmental vibrations of different amplitudes and frequencies. The experiments reveal that each volt of waveform strain generated by the AWG and PZT corresponds to a phase response of 9.65 rad/V. The phase results obtained from the Φ-OTDR system are fitted to the known frequency and amplitude sinusoidal signals. The fitted sinusoidal signal serves as the ideal phase waveform. By comparing the differences between the phase results and the fitted sinusoidal signal, the fidelity of the system's restoration of environmental vibrations was quantitatively described using the root mean square error (RMSE) [32]. The RMSE is calculated by the root mean square difference between the fitted sinusoidal signals and the phases results. A higher RMSE value indicates a larger phase error in the process

Optics EXPRESS

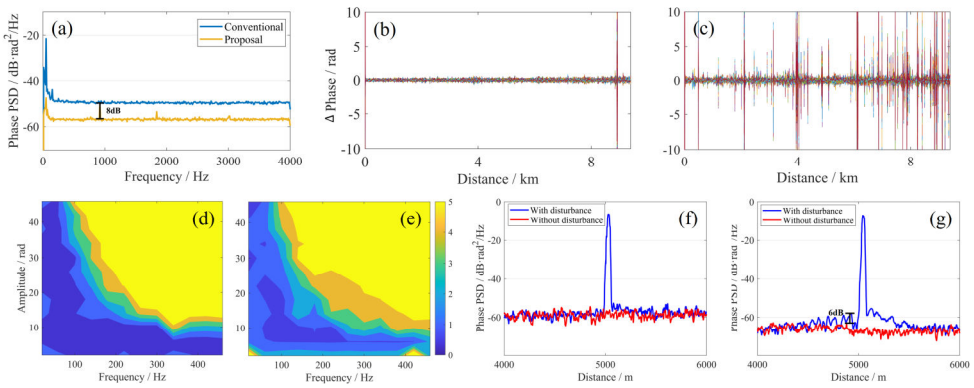

Fig. 9. The performance of the Φ-OTDR with self-mixing interferometry and triple-frequency structure without on-line EDFA including (a) the phase noise floor, the consecutive phase traces along the FUT using (b) triple-frequency scheme and (c) single-frequency scheme, the dynamic range of (d) proposal structure and (e) conventional structure, the spatial crosstalk (f) without on-line EDFA and (g) with on-line EDFA.

of phase mapping vibrations. Figure 9(d) and (e) present the RMSE values for Φ-OTDR with the proposal scheme and the conventional scheme. The bluer the color block, the smaller the RMSE value is. The change of the color block from blue to yellow indicates an increase in the error between the phases and the vibrations. When the amplitudes and frequencies of the vibrations increase to a certain degree, due to the unwrapping problems or others, the RMSE becomes large and is shown in the yellow area. Observing the demarcation of the RMSE color block from blue to yellow, the amplitudes and frequencies of vibrations that can be restored by Φ-OTDR using self-mixing interferometry or conventional structure are similar. It reveals that the amplitude-frequency characteristic for high frequencies and large amplitudes is not affected by the different structures. By referring to the lower left part of Fig. 9(d) and (e), it can be observed that the Φ-OTDR system using self-mixing interferometry yields a smaller phase error to the vibration. Based on the mitigation of laser phase noise, Φ-OTDR using self-mixing interferometry has a better amplitude-frequency characteristic for low frequencies and small amplitudes compared to the conventional scheme.

Furthermore, the PSD is calculated along the range of 2 km around the PZT at the location of 5 km to inspect the spatial crosstalk as given in Fig. 9(f) and (g). The PSD results of the vibration frequency during 4 seconds are averaged along the FUT. The PSD results with the disturbance is outline by the blue curve and the PSD results without the disturbance is outline by the red curve. The spatial crosstalk is characterized by difference between the PSD with disturbance and without disturbance around the position of PZT. The spatial crosstalk of the scheme without on-line EDFA is shown in Fig. 9(f) and the crosstalk of the scheme with on-line EDFA is shown in Fig. 9(g). It is observed that, before and after the PZT for the system without on-line EDFA, there is no significant difference in PSD with and without disturbance. In comparison, at the position close to the PZT, the PSD of the system with on-line EDFA increase by more than 6 dB compared to the case without disturbance. This indicates that the crosstalk of system can be effectively reduced by improving the extinction ratio (ER) without the introduction of amplifier spontaneous emission (ASE) noise by the EDFA [33]. Although the absence of on-line EDFA results in the decrease in power and SNR leading to the increase in the noise floor, the system can be optimized from the performance of spatial crosstalk.

Optics EXPRESS

5. Conclusion

This paper introduces a cost-effective Φ-OTDR system that leverages self-mixing interferometry for mitigating laser phase noise and triple-frequency detection for suppressing interference fading noise. The innovative approach employs a fixed-wavelength DFB-SL with a 93 kHz linewidth, realizing long-distance detection up to 40 km without fading noise. Compared to the conventional scheme, the proposed scheme achieves 8 to 22 dB mitigation of noise floor within a range of 35 km. Leveraging the high-power characteristic of the DFB-SL, the proposed scheme achieves fading-free detection over 10 km without the need for an on-line EDFA. The study discussed the performances of the scheme, including the noise floor, interference fading noise, amplitude-frequency characteristic, and spatial crosstalk. Based on the experimental results, the system proposed in this work provides a cost-effective solution for laser phase noise mitigation, particularly in scenarios where on-line amplifiers cannot be integrated.

Funding. Guangdong S&T Programme (2024B0101030001); National Natural Science Foundation of China (U2001601, U22A2087); in part by Project supported by Southern Marine Science and Engineering Guangdong Laboratory(Zhuhai) (SML2023SP231); Special Project for Marine Economy Development of Guangdong Province (GDNRC [2024]16).

Disclosures. The authors declare no conflicts of interest.

Data availability. Data underlying the results presented in this paper are not publicly available at this time but may be obtained from the authors upon reasonable request.

References

1. Z. Wang, B. Lu, Q. Ye, *et al.*, "Recent progress in distributed fiber acoustic sensing with Φ-OTDR," Sensors **20**(22), 6594 (2020).
2. Z. Wu, H. Zhang, P. P. Shum, *et al.*, "Supermode Bragg grating combined Mach-Zehnder interferometer for temperature-strain discrimination," Opt. Express **23**(26), 33001–33007 (2015).
3. S. Chen, J. Han, Q. Sui, *et al.*, "Advanced Signal Processing in Distributed Acoustic Sensors Based on Submarine Cables for Seismology Applications," J. Lightwave Technol. **41**(13), 4164–4175 (2023).
4. F. Sigmundsson, A. Hooper, and S. Hreinsdóttir, "Segmented lateral dyke growth in a rifting event at Bárðarbunga volcanic system, Iceland," Nature **517**(7533), 191–195 (2015).
5. P. Jousset, G. Currenti, B. Schwarz, *et al.*, "Fibre optic distributed acoustic sensing of volcanic events," Nat. Commun. **13**(1), 1753 (2022).
6. N. Lalam, P. Westbrook, K. Naeem, *et al.*, "Pilot-scale testing of natural gas pipeline monitoring based on phase-OTDR and enhanced scatter optical fiber cable," Sci. Rep. **13**(1), 14037 (2023).
7. J. T. Li, B. Chang, J. T. Du, *et al.*, "Coherently parallel fiber-optic distributed acoustic sensing using dual Kerr soliton microcombs," Sci. Adv. **10**(3), 8666 (2024).
8. S. Nikitin, E. Fomiryakov, D. Kharasov, *et al.*, "Characterization of Ultra-Narrow Linewidth Lasers for Phase-Sensitive Coherent Reflectometry Using EOM Facilitated Heterodyning," J. Lightwave Technol. **38**(6), 1446–1453 (2020).
9. Y. Shao, H. Liu, P. Peng, *et al.*, "Distributed vibration sensor with laser phase-noise immunity by phase-extraction Φ-OTDR," Photonic Sens. **9**(3), 223–229 (2019).
10. B. G. Gorshkov, A. E. Alekseev, D. E. Simikin, *et al.*, "A cost-effective distributed acoustic sensor for engineering geology," Sensors **22**(23), 9482 (2022).
11. B. G. Gorshkov, A. E. Alekseev, M. A. Taranov, *et al.*, "Low noise distributed acoustic sensor for seismology applications," Appl. Opt. **61**(28), 8308–8316 (2022).
12. Z. Xiao, J. Chen, Y. Deng, *et al.*, "Signal-and-Kernel Phase Noise Compensation Method for Distributed Acoustic Sensors," J. Lightwave Technol. **42**(18), 3396649 (2024).
13. X. He, S. Xie, F. Liu, *et al.*, "Multi-event waveform-retrieved distributed optical fiber acoustic sensor using dual-pulse heterodyne phase-sensitive OTDR," Opt. Lett. **42**(3), 442–445 (2017).
14. Y. Shan, W. Ji, X. Dong, *et al.*, "An Enhanced Distributed Acoustic Sensor Based on UWFBG and Self-Heterodyne Detection," J. Lightwave Technol. **37**(11), 2700–2705 (2019).
15. X. He, M. Zhang, S. Xie, *et al.*, "Identification and observation of the phase fading effect in phase-sensitive OTDR," OSA Continuum **1**(3), 963–970 (2018).
16. S. Liu, L. Shao, F. Yu, *et al.*, "Quantitative demodulation of distributed low-frequency vibration based on phase-shifted dual-pulse phase-sensitive OTDR with direct detection," Opt. Express **30**(6), 10096–10109 (2022).
17. X. Wang, B. Lu, Z. Wang, *et al.*, "Interference-Fading-Free Φ-OTDR Based on Differential Phase Shift Pulsing Technology," IEEE Photonics Technol. Lett. **31**(1), 39–42 (2019).
18. J. Jiang, Z. Wang, Z. Wang, *et al.*, "Continuous chirped-wave phase-sensitive optical time domain reflectometry," Opt. Lett. **46**(3), 685–688 (2021).

Optics EXPRESS

19. M. Zabihi, Y. Chen, T. Zhou, *et al.*, "Continuous Fading Suppression Method for Φ-OTDR Systems Using Optimum Tracking Over Multiple Probe Frequencies," J. Lightwave Technol. **37**(14), 3602–3610 (2019).
20. G. Tu, M. Zhao, Z. Tang, *et al.*, "Fading Noise Suppression in Φ-OTDR Based on Nearest Neighbor Analysis," J. Lightwave Technol. **38**(23), 6691–6698 (2020).
21. Q. Yuan, F. Wang, T. Liu, *et al.*, "Compensating for influence of laser-frequency-drift in phase-sensitive OTDR with twice differential method," Opt. Express **27**(3), 3664–3671 (2019).
22. X. He, M. Zhang, L. Gu, *et al.*, "Performance improvement of dual-pulse heterodyne distributed acoustic sensor for sound detection," Sensors **20**(4), 999 (2020).
23. S. Wang, X. Fan, Q. Liu, *et al.*, "Distributed fiber-optic vibration sensing based on phase extraction from time-gated digital OFDR," Opt. Express **23**(26), 33301–33309 (2015).
24. H. Qian, B. Luo, H. He, *et al.*, "Phase Demodulation Based on DCM Algorithm in Φ-OTDR With Self-Interference Balance Detection," IEEE Photonics Technol. Lett. **32**(8), 473–476 (2020).
25. Z. Hu, Y. Tang, S. Yang, *et al.*, "A new phase demodulation method for φ-OTDR based on coherent detection," Optics Frontiers Online 2020: Distributed Optical Fiber Sensing Technology and Applications **11607**, 33–131 (2021).
26. X. Zhou, Y. Gao, J. Huo, *et al.*, "Theoretical Analysis of Phase Noise Induced by Laser Linewidth and Mismatch Length in Self-Homodyne Coherent Systems," J. Lightwave Technol. **39**(5), 1312–1321 (2021).
27. M. J. O'mahony and I. D. Henning, "Semiconductor laser linewidth broadening due to 1/f carrier noise," Electron. Lett. **19**(23), 1000–1001 (1983).
28. Y. Wakisaka, D. Iida, H. Oshida, *et al.*, "Fading Suppression of Φ-OTDR With the New Signal Processing Methodology of Complex Vectors Across Time and Frequency Domains," J. Lightwave Technol. **39**(13), 4279–4293 (2021).
29. J. Li, H. Liu, Y. Xiao, *et al.*, "Fully and wideband distributed acoustic sensing with high sensitivity by an air-ring microstructure optical fiber," J. Lightwave Technol. **Early Access**, 3515082 (2025).
30. Y. Wu, Z. Wei, T. Li, *et al.*, "Three-Layer Structure Multiplexing Fading Elimination Method in Long-Haul Φ-OTDR," J. Lightwave Technol. **42**(14), 3383413 (2024).
31. Y. Xiao, H. Liu, J. X. Shen, *et al.*, "Fading suppression and noise reduction of a DAS system integrated multi-core fiber," Opt. Express **32**(15), 26793–26807 (2024).
32. T. Wang, J. Zhang, Z. Ma, *et al.*, "Comparison of Amplitude-Frequency Response Characteristics Between DCM and Arctan Algorithms in ϕ-OTDR," J. Lightwave Technol. **41**(20), 6608–6614 (2023).
33. Z. Cheng, X. Shu, L. Ma, *et al.*, "On-chip silicon electro-optical modulator with ultra-high extinction ratio for fiber-optic distributed acoustic sensing," Nat. Commun. **14**(1), 7409 (2023).